Laplace field microscopy for label-free imaging of dynamic biological structures

Taewoo Kim and Gabriel Popescu*

Quantitative Light Imaging Laboratory, Department of Electrical and Computer Engineering, Beckman Institute for Advanced Science & Technology, University of Illinois at Urbana-Champaign, Urbana, Illinois 61801, USA

**Corresponding author: gpopescu@illinois.edu*

Received September 1, 2011; revised November 1, 2011; accepted November 1, 2011; posted November 2, 2011 (Doc. ID 153898); published December 1, 2011

We present Laplace field microscopy as a method for generating intrinsic contrast of transparent specimens. This technique uses a spatial light modulator to perform the Laplacian of the field in the Fourier plane of a microscope image. The resulting image incorporates phase information and thus renders high contrast images from phase objects. We demonstrate the potential of the method by imaging index-matched beads, unlabeled tissue slices, and dynamic live cells. © 2011 Optical Society of America

OCIS codes: 170.0180, 170.1530, 170.1650, 170.6935.

Unlabeled cells and tissues are transparent under visible light and, as such, can be approximated as *phase* objects, with a transmission function of the form $t(x,y) \simeq A\exp[i\phi(x,y)]$. Accordingly, the *intensity* image, as rendered by a bright field microscope, loses the phase information and yields negligible contrast, i.e., $I = A^2$, which is independent of (x,y). Much of light microscopy's four-century history has been shaped by the quest of developing new contrast mechanisms [1,2]. In particular, *intrinsic contrast* methods exploit the light-tissue interaction in such a way as to couple the information carried by the phase into the final intensity image. Note that these techniques do not aim to provide quantitative information about the optical thickness of the specimen. Instead, they provide noninvasive, label-free access to microscopic structures of cells and tissues, without the restrictions associated with exogenous contrast agents. Recently, a number of differential-phase methods have been proposed [3–9]. However, the most commonly used label-free methods are phase contrast (PC) microscopy [10] and differential interference contrast (DIC) microscopy [11], which have been playing a major role in biological investigations for several decades.

While extremely powerful, these methods suffer from optical artifacts: *halos* in the case of PC and *shadows* in DIC. In particular, DIC provides an intensity image that is related to the *gradient* of the field. Thus, using birefringent optics, two identical replicas of the image field, slightly shifted transversely, are produced at the observation plane

$$\begin{aligned} I(x,y) &= A|e^{i\phi(x,y)} + e^{i[\phi(x+\delta x,y)+\alpha]}|^2 \\ &= 2A\{1+\cos[\delta\phi_x(x,y)+\alpha]\}. \end{aligned} \tag{1}$$

In Eq. (1), I is the image intensity, ϕ the phase of the object, δx is the transverse shift between the two images, α is a controllable phase shift between the two fields, and the phase shift between the two fields, $\delta\phi$, is proportional to the 1D gradient of the phase ϕ:

$$\delta\phi_x(x,y) = \phi(x+\delta x,y) - \phi(x,y) \qquad \propto \frac{\partial\phi(x,y)}{\partial x}. \tag{2}$$

DIC is extremely powerful in revealing fine details in the specimen because adjusting α to a value of $-\pi/2$ transforms the cosine in Eq. (1) into a sine, $\cos[\delta\phi_x(x,y) - \pi/2] = \sin[\delta\phi_x(x,y)]$, which for small values of $\delta\phi$ becomes proportional to the 1D gradient of the phase $\sin[\delta\phi_x(x,y)] \simeq \delta\phi_x(x,y)$. Therefore, DIC is highly sensitive to edges and renders beautiful images of fibrous structures, for example. However, its limitation comes from the fact that the first-order derivative changes sign rapidly across an edge, which generates spurious bright and dark regions ("shadowing") along the direction of the gradient.

Here we present a differential-phase method that conserves the benefits of DIC, rendering high contrast images of transparent specimens, while at the same time suppressing the artifacts. Our technique, referred to as *Laplace field microscopy* (*LFM*), carries the spirit of DIC in the sense that it produces an intensity distribution that incorporates phase information. However, because the LFM image relates to the Laplacian of the field, which has a scalar output, the image does not suffer from directional artifacts. Recently it was found that the Laplacian of a quantitative phase image is superior to the gradient and, thus, holds great potential for biological investigation [12]. Essentially, the LFM introduced here is a method for obtaining the Laplacian of the field directly, without requiring first to measure a quantitative phase image.

The experimental setup is described in Fig. 1. The LFM is designed as an additional module, attached to an existing inverted microscope, which itself is unmodified. The white light from a halogen lamp is spatially filtered to achieve full spatial coherence. This collimated field is used for illuminating the specimen in transmission. The transmitted light is collected by the objective and the image is formed at the output port via the tube lens (TL). The LFM module consists of a $4f$ imaging system that contains an amplitude spatial light modulator (SLM) at the Fourier plane and achromatic doublets to avoid color aberrations. Thus, lens L_1 generates the Fourier transform of the image field, $\tilde{U}(k_x,k_y)$. Note that, although broadband, the autocorrelation of the field has a well-defined modulation (mean) frequency, with respect to which the Fourier transform is well defined. [12,13].

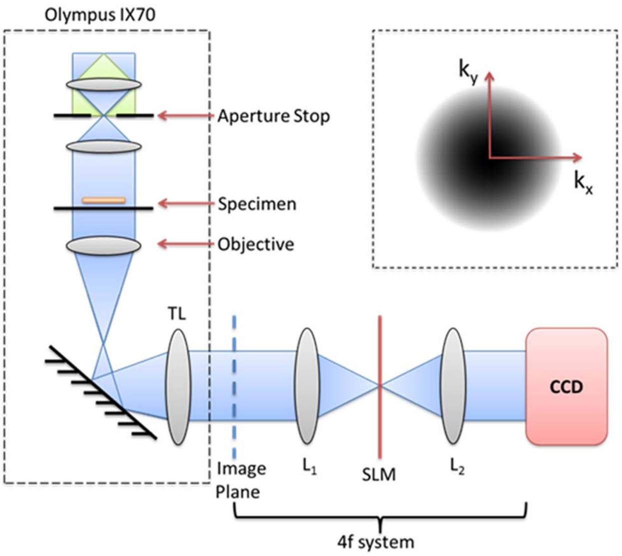

Fig. 1. (Color online) LFM setup built as a module added on to Olympus IX70 bright field microscope. L_1 and L_2 has focal length of 75 mm and 150 mm, respectively. Inset: parabola modulation profile on SLM.

The SLM introduces an amplitude filter of the parabolic form, $H(k_x, k_y) = a(k_x^2 + k_y^2)$, with a denoting a constant. The DC component of the scattered light is strongly attenuated through this parabolic filter, while the scattered AC component experiences progressively less attenuation toward higher frequencies. The SLM is obtained from an Epson Powerlite S5 projector with a contrast ratio of 400/1. The SLM pixel size ($p = 13\,\mu$m) limits the resolution in k-space, δk, and, thus, the field of view at the image plane over which the modulation produced by one SLM pixel is uniform. In our setup, $\delta k = k_0 p/f$, where $k_0 = 2\pi/\lambda$ and $f = 150$ mm is the focal length of L_2. This field of view in the image plane is of the order of $2\pi/\delta k \sim 6.25$ mm. However, we successfully obtained high contrast images over the entire CCD, which is larger, 13 mm on the side.

The lens L_2 Fourier transforms the field back to the image domain, such that at the CCD plane we obtain

$$U_i(x,y) = a\Im[(k_x^2 + k_y^2)\tilde{U}(k_x, k_y)] = -a\nabla^2 U(x,y). \quad (3)$$

For phase objects, i.e., $U(x,y) \simeq A\exp[i\phi(x,y)]$, under the Born approximation, the intensity image reveals directly the first- and second-order derivatives of the phase itself. Note that the CCD records the intensity distribution, $I(x,y) = |U_i(x,y)|^2$:

$$I(x,y) \propto [\nabla^2\phi(x,y)]^2 + \left[\left(\frac{\partial\phi(x,y)}{\partial x}\right)^2 + \left(\frac{\partial\phi(x,y)}{\partial y}\right)^2\right]^2. \quad (4)$$

Thus, Eq. (4) establishes that LFM reveals high contrast images from entirely transparent (phase) structures.

In order to demonstrate this capability of LFM, first we imaged $3\,\mu$m beads immersed in oil, which exhibit low contrast under bright field illumination [Fig. 2(a)]. When the parabolic amplitude filter is turned on, the contrast of the bead increases significantly, as illustrated in Figs. 2(b) and 2(c). Figure 2(c) shows the profiles through the two images. We used Eq. (4) particularized for the case of the spherical particle, where the phase shift is $\phi(x) = 2k_0[R^2 - x^2]^{1/2}$, with R the particle radius, x the horizontal distance from the bead center, and $k_0 = 2\pi/\lambda$. In order to fit the experimental profile and also include the effects of finite resolution, first we convolved the phase shift function which essentially represents the propagating field with a Gaussian function of root mean square . width given by the diffraction limit, i.e., $\lambda/2\,\mathrm{NA} = 0.2\,\mu$m for $\lambda = 0.53$ nm. Note that the derivatives in Eq. (4) associated with this phase distribution diverge at $x = \pm R$; thus, we performed the convolution integral in a principle value sense, avoiding the singularity points. Using this new phase profile, Eq. (4) was numerically evaluated as shown in Fig. 2. The second-order derivative (curvature) of the phase takes the significant role in this spherically shaped object case. This profile clearly shows that LFM is very sensitive to edges, without introducing directional artifacts that plague DIC. On the other hand, the bright field image shows a flat profile, indicating low contrast, as expected.

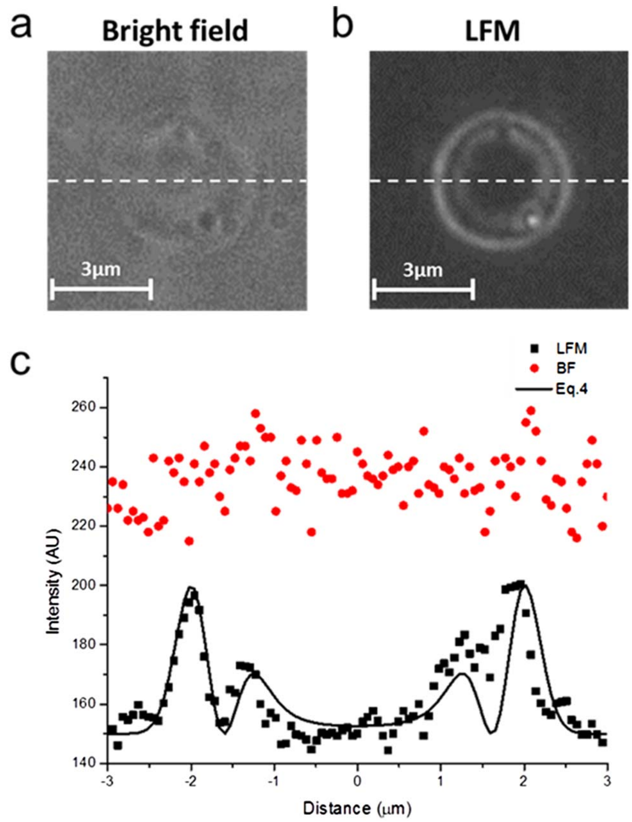

Fig. 2. (Color online) $3\,\mu$m polystyrene beads ($n = 1.59$) immersed in oil ($n = 1.516$) measured with bright field and LFM. (a) Bright field (BF) image of the bead. (b) LFM image of the bead. (c) Horizontal profile of each measurement (scatters) and simulated result using Eq. (4).

LFM can be used to study unstained tissues sections. Figure 3 shows a side-by-side comparison of bright field and LFM images obtained from the same field of view of gut and kidney sections. The gain in contrast using LFM is significant and enables us to distinguish specific morphologic structures that are typically studied using various stains. The gain in contrast is well represented

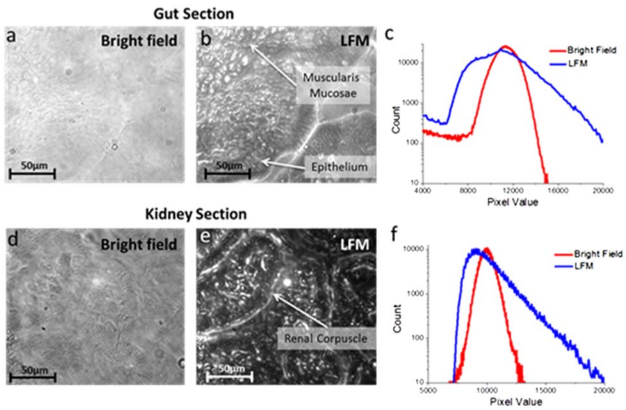

Fig. 3. (Color online) Bright field and LFM images of tissue samples. (a), (b) Images of gut section taken with BF and LFM. (c) Histogram of (a) and (b) (semilog plot). (d), (e) Images of kidney section taken with BF and LFM. (e) Histogram of (d) and (e) (semilog plot).

by the intensity histograms, which clearly become much broader in LFM than in bright field [Fig. 3(c) and 3(f)].

An important feature of LFM is that it can acquire images as fast as the camera allows. Thus, it is suitable for studying highly dynamic specimen such as cells. Figure 4 shows time-resolved imaging of HeLa cells in culture. Cells were prepared with 40% confluency in a 35 mm glass bottom dish containing culture medium F-12 K (Kaighn's modification of Ham's F-12 with L-glutamine). After passaging, we left the cells in the incubator for three hours so they can attach to the bottom and grow. Once attached to the substrate, the HeLa cells are very transparent [Fig. 4(a)]. However, in LFM the cell boundary and internal structures (e.g., nucleus, other organelles) are clearly resolved. Figure 4(c) shows the time sequence over 35 minutes, in which the cell rounds up.

We would like to note here an interesting aspect of studying dynamics using certain derivatives of the spatial phase distribution rather than the quantitative phase image itself. It has been already shown that, since this optical pathlength contains information about both thickness and refractive index of the specimen (see, e.g. Chapter 15 in [14]), quantitative phase imaging is capable of investigating both *out-of-plane* cell membrane fluctuations (using the thickness component) [15,16] and

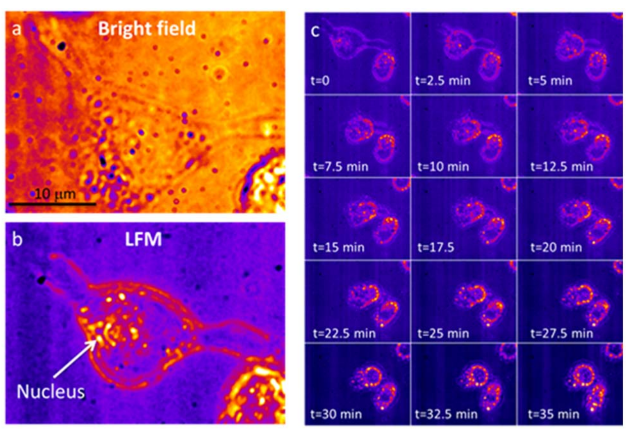

Fig. 4. (Color online) (a) Bright field image of a HeLa cell. (b) LFM image of the same cell as in (a), but a few minutes later. (c) Dynamic measurement of a HeLa cell using LFM.

in-plane intracellular transport (using the refractive index component) [17,18].

The data analysis is based on the *dispersion relation* that connects the temporal and spatial frequencies of the fluctuations. This relation is obtained directly from the differential equations that govern the motions (e.g., the diffusion equation in the case of Brownian particle transport). This means that, for studying dynamics, we do not need to know the phase shift quantitatively; rather, one of its derivatives is sufficient. We anticipate that LFM and similar approaches will allow for novel investigations of dynamic systems, while bringing great simplifications in the optical setup.

In summary, we introduced LFM as a differential-phase method using a spatial light modulation. LFM shows its advantage over other differential-phase method by removing the directional shadow artifact, while preserving the high contrast coming from the edges of samples. Furthermore, LFM shows its capability of fast measurement in dynamic samples.

This research was supported by the National Science Foundation (NSF) (grants CBET 08-46660 CAREER, CBET-1040462 MRI) and National Cancer Institute (R21 CA147967-01). TK acknowledges help with HeLa cell preparation from Shamira Sridharan and Ryan Tapping. For more information, visit http://light.ece.uiuc.edu/.

References

1. M. Pluta, *Advanced Light Microscopy* (Polish Scientific Publishers, Warszawa, 1988).
2. Nat. Cell Biol. **11**, 1165 (2009).
3. D. K. Hamilton and C. J. R. Sheppard, J. Microsc. **133**, 27 (1984).
4. T. Wilson, Optik **80**, 167 (1988).
5. C. K. Hitzenberger and A. F. Fercher, Opt. Lett. **24**, 622 (1999).
6. C. Rylander, T. E. Milner, K. R. Diller, and A. J. Welch, Lasers Surg. Med. **32**, 5(2003).
7. M. Lew, X. Q. Cui, X. Heng, and C. H. Yang, Opt. Lett. **32**, 2963 (2007).
8. C. H. Yang, A. Wax, I. Georgakoudi, E. B. Hanlon, K. Badizadegan, R. R. Dasari, and M. S. Feld, Opt. Lett. **25**, 1526 (2000).
9. A. Ahn, C. H. Yang, A. Wax, G. Popescu, C. Fang-Yen, K. Badizadegan, R. R. Dasari, and M. S. Feld, Appl. Opt. **44**, 1188 (2005).
10. F. Zernike, Science **121**, 345 (1955).
11. G. Nomarski, J. Phys. Radium **16**, 9S (1955).
12. Z. Wang, L. J. Millet, M. Mir, H. Ding, S. Unarunotai, J. A. Rogers, M. U. Gillette, and G. Popescu, Opt. Express **19**, 1016 (2011).
13. Z. Wang and G. Popescu, Appl. Phys. Lett. **96**, 051117 (2010).
14. G. Popescu, *Quantitative Phase Imaging of Cells and Tissues* (McGraw-Hill, New York, 2011).
15. Y. K. Park, C. A. Best, T. Kuriabova, M. L. Henle, M. S. Feld, A. J. Levine, and G. Popescu, Phys. Rev. E **83**, 051925 2011).
16. Y. K. Park, C. A. Best, K. Badizadegan, R. R. Dasari, M. S. Feld, T. Kuriabova, M. L. Henle, A. J. Levine, and G. Popescu, Proc. Nat. Acad. Sci. **107**, 6731 (2010).
17. Z. Wang, L. Millet, V. Chan, H. Ding, M. U. Gillette, R. Bashir, and G. Popescu, J. Biomed. Opt. **16**, 026019 (2011).
18. R. Wang, Z. Wang, J. Leigh, N. Sobh, L. Millet, M. U. Gillette, A. J. Levine, and G. Popescu, J. Phys. Condens. Matter **23**, 374107 (2011).